Environ Monit Assess (2012) 184:3813–3829
DOI 10.1007/s10661-011-2226-0

A comparison of radiometric correction techniques in the evaluation of the relationship between LST and NDVI in Landsat imagery

Kok Chooi Tan · Hwee San Lim · Mohd Zubir MatJafri · Khiruddin Abdullah

Received: 25 January 2011 / Accepted: 30 June 2011 / Published online: 15 July 2011
© Springer Science+Business Media B.V. 2011

Abstract Atmospheric corrections for multi-temporal optical satellite images are necessary, especially in change detection analyses, such as normalized difference vegetation index (NDVI) rationing. Abrupt change detection analysis using remote-sensing techniques requires radiometric congruity and atmospheric correction to monitor terrestrial surfaces over time. Two atmospheric correction methods were used for this study: relative radiometric normalization and the simplified method for atmospheric correction (SMAC) in the solar spectrum. A multi-temporal data set consisting of two sets of Landsat images from the period between 1991 and 2002 of Penang Island, Malaysia, was used to compare NDVI maps, which were generated using the proposed atmospheric correction methods. Land surface temperature (LST) was retrieved using ATCOR3_T in PCI Geomatica 10.1 image processing software. Linear regression analysis was utilized to analyze the relationship between NDVI and LST. This study reveals that both of the proposed atmospheric correction methods yielded high accuracy through examination of the linear correlation coefficients. To check for the accuracy of the equation obtained through linear regression analysis for every single satellite image, 20 points were randomly chosen. The results showed that the SMAC method yielded a constant value (in terms of error) to predict the NDVI value from linear regression analysis-derived equation. The errors (average) from both proposed atmospheric correction methods were less than 10%.

Keywords Landsat · NDVI · SMAC · LST

K. C. Tan (✉) · H. S. Lim · M. Z. MatJafri · K. Abdullah
School of Physics, Universiti Sains Malaysia,
11800 Penang, Malaysia
e-mail: kokchooi86@gmail.com

H. S. Lim
e-mail: hslim@usm.my

M. Z. MatJafri
e-mail: mjafri@usm.my

K. Abdullah
e-mail: khirudd@usm.my

Introduction

Satellite image analysis has provided invaluable data for environment monitoring over the past few decades. Repeat observations of a given study area with spatial synchronization increases the quality of environmental observation data, especially in change detection analysis (Janzen et al. 2006; Du et al. 2002). However, there is variation in the sensor's response over time due to changes in satellite sensor calibration, variation in atmospheric effects, changes in target reflectance, and differences in illumination and observation angles (Eckhardt et al. 1990).

Two levels of radiometric correction, namely absolute and relative, have been widely applied in change detection analysis. Absolute radiometric cor-

rection requires either an atmospheric correction algorithm or both atmospheric models and the related atmospheric properties at the image acquisition time. This allows for the conversion of the digital number of a pixel to the percent of reflectance at the surface of Earth (Richter 1990; Song et al. 2001). Many studies have been carried out to improve the removal of the scattering and absorption caused by atmospheric effects. The obtained results from these studies have been used to generate the atmospheric transfer code for atmospheric correction purposes (Kaufman 1988). Although a fair amount of research focuses on radiative transfer module, the atmospheric profile and the atmospheric and sensor properties at the time of image acquisition are still required. Thus, a problem exists when implementing absolute radiometric correction, due to the difficulty in acquiring atmospheric properties for the particular satellite images (Canty et al. 2004). Furthermore, for most historical satellite images, such data are not readily available. This becomes the major obstacle for the application of radiative transfer module in radiometric correction.

Inversely, alternative methods for radiometric correction are available through a variety of relative radiometric correction techniques when atmospheric profiles are not available. Relative radiometric correction involves a simpler theory regarding atmospheric profiles and less computationally intensive. A variety of relative radiometric correction techniques have been developed for multi-temporal satellite images (Du et al. 2002; Furby and Campbell 2001). Among these techniques, relative radiometric normalization has been widely used in many studies. It generates data that are normalized for multi-spectral and multi-temporal images taken under different conditions. In addition, all of the atmospheric parameters and sensor calibration procedures that are compulsory for the use of absolute radiometric correction methods are not necessary for relative radiometric normalization. Procedures involve examining two or more multi-temporal satellite images through the relationship between top of atmosphere (TOA) or surface reflectance of the same study area. It assumed that the reflectance value is consistent for the images within the study period and can be well-approximated by a linear function (Canty et al. 2004). The difficulty encountered in the application of the relative radiometric normalization technique is choosing suitable and proper pseudo-invariant features (PIF). Any selection of improper PIF may introduce error into the obtained results after normalization.

The main purpose of radiometric correction is to remove variation in the sensor's response to every target in multi-temporal satellite images. The selection of an appropriate radiometric correction method, which is matched with the study's purpose, can yield accurate results after correction.

Study area

Penang Island is located in the northern part of Malaysia, within latitudes 5° 12′N to 5° 30′ N and longitudes 100° 09′ E to 100° 26 E (Fig. 1). George Town is the capital city of the state of Penang and is also the second-largest city in Malaysia. It is located in the eastern region of Penang Island. Additionally, Penang Island is the most populated island in the country, with an estimated population of 720,000 and an area of approximately 295 km^2.

Normally, Penang Island experiences a warm and sunny equatorial climate throughout the entire year (Tan et al. 2010). The average annual temperature varies between 27°C and 30°C, and the mean daily temperature is about 27°C. The average annual relative humidity ranges between 70% and 90%. The average annual rainfall is about 267 cm, though the annual total can be as high as 624 cm (Ahmad et al. 2006). During the period of monsoon winds, weather conditions change drastically. Specifically, there is sunshine during the day but rainfall in the evenings.

Penang Island consists primarily of hilly terrain, with the highest point being Western Hill (part of Penang Hill) at about 830 m above sea level. The terrain is mostly comprised of coastal plains, hills, and mountains. The coastal plains are narrow; the most extensive ones are located in the northeast and form a triangular promontory where George Town is located.

Remotely sensed data

Two Landsat images, acquired on January 11, 1991 (Landsat 5 TM) and January 17, 2002 (Landsat ETM +), were used for this study. Both of these satellite images met the basic criteria that are necessary to

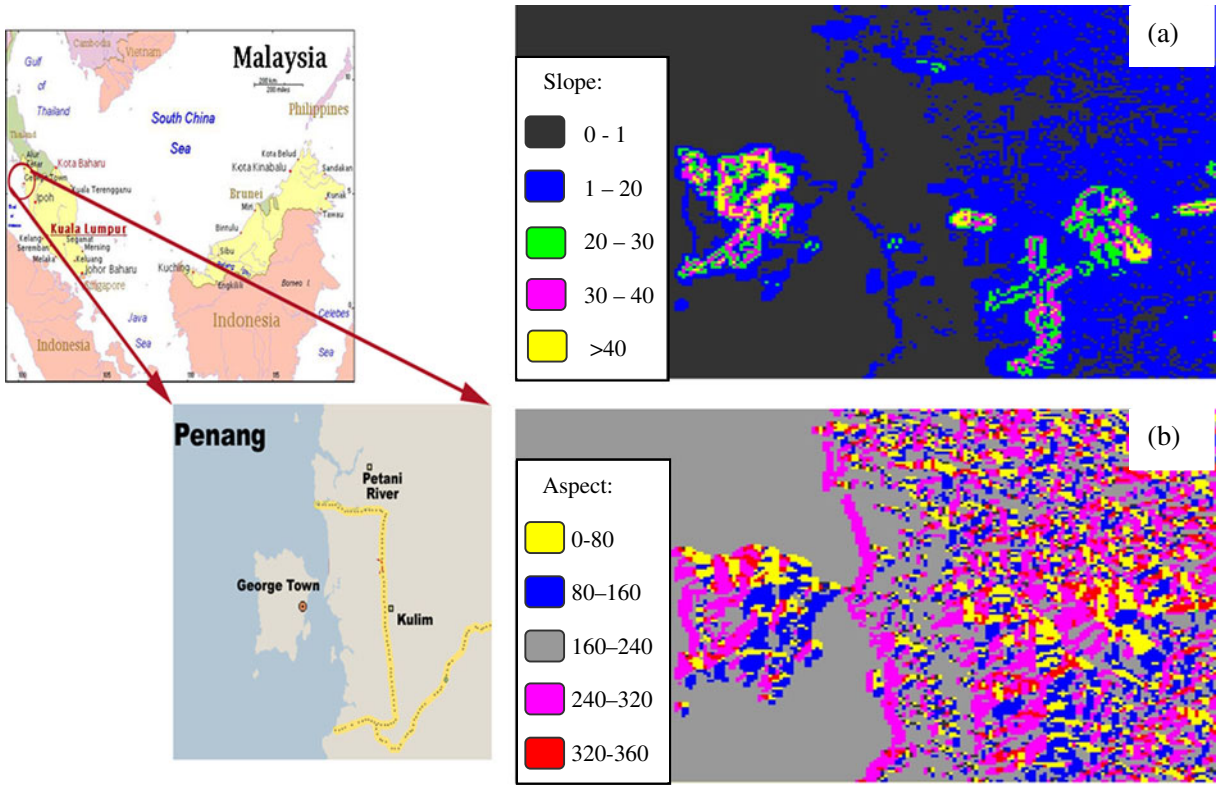

Fig. 1 The geographical features of the study area, input thematic layers: **a** slope, **b** aspect

obtain accurate results, including long time series availability and less than 10% cloud cover over the total study area (Sun et al. 2008). Since Penang Island is located at the equatorial region, it was impossible to acquire the Landsat images without any cloud coverage in the study area. The study areas are entirely contained within path 128, and row 56.

Methodology

Image pre-processing

Using multi-temporal satellite images in change detection analysis necessitated that all of the satellite images be co-registered in the same coordinate system (Chen et al. 2006). This ensures that the detection of change for every pixel can be analyzed accurately. For example, sometimes normalized difference vegetation index (NDVI) analysis is based on a pixel-by-pixel analysis. Thus, every single pixel for both satellite images should match with one another to accurately obtain the desired results. In co-registered images, RMSE (root mean-square error) provides a good indicator to measure accuracy. RMSE values of less than 0.5 pixels indicate that the coordinates are adequately co-registered for Landsat images (Lunetta and Elvidge 1998). If the RMSE is greater than one pixel, it can result in misinterpretations in change detection analysis of satellite images at the same pixel (Sun et al. 2008). Using PCI Geomatica 10.1 image processing software, both satellite images were resampled to 30 m pixel size. Then, they were georectified using second-order polynomial equations with the nearest neighbor method. Overall, both satellite images were associated with RMSE values of less than 0.5 pixels in this study (Vicente-Serrano et al. 2008; Schroeder et al. 2006; Kabbara et al. 2008).

Radiometric calibration

The problem of non-homogeneity is common in working with multi-temporal satellite images. This issue affects the analysis of abrupt change in vegetation cover (Vicente-Serrano et al. 2008). Prob-

lems with heterogeneity are mainly caused by absorption and scattering effects from aerosol particles and gases traveling to the Earth and back to the sensor itself. In addition, they can also be caused by noise from the surface signals. Furthermore, atmospheric effects may introduce error into obtained results due to misinterpretation of the satellite images (Tokola et al. 1999). Therefore, sensor calibration should be done when analyzing change detection, especially in NDVI.

In radiometric calibration, a precise conversion of the digital number (DN) for Landsat images to satellite radiance units (L) (Mather 2004; Vicente-Serrano et al. 2008; Chander et al. 2009a) is possible by using the following equation:

$$L_\lambda = \left(\frac{LMAX_\lambda - LMIN_\lambda}{Q_{calmax} - Q_{calmin}}\right)(Q_{cal} - Q_{calmin}) + LMIN_\lambda \quad (1)$$

where

L_λ	Spectral radiance at the sensor's aperture, W m^{-2} sr^{-1} μm^{-1}.
$LMAX_\lambda$	Spectral radiance scaled to Q_{calmax}, W m^{-2} sr^{-1} μm^{-1}.
$LMIN_\lambda$	Spectral radiance scaled to Q_{calmin}, W m^{-2} sr^{-1} μm^{-1}.
Q_{calmax}	Maximum quantized calibrated pixel value (DN=255) corresponding to $LMAX_\lambda$.
Q_{calmin}	Minimum quantized calibrated pixel value (DN=0) corresponding to $LMIN_\lambda$.
Q_{cal}	Quantized calibrated pixel value [DN].

All related constants were obtained through the study done by Chander et al. (2009b).

Then, the obtained value of radiance was converted to a TOA reflectance value according to Chander et al. (2009b),

$$\rho = \frac{\pi L d^2}{ESun_\lambda \cos\theta} \quad (2)$$

where ρ is the TOA reflectance for band λ, d is the Earth–Sun distance in astronomical units, ESunλ is the mean solar-exoatmospheric irradiance for band λ, and θ is the solar zenith angle in degrees. ESunλ values were obtained from Chander and Markham (2003) for the TM image, and from the Landsat-7 Science Data User Handbook for the ETM+ image. The advantage of TOA reflectance is that it can normalize the sensor by taking into account different solar zenith angles at the different times and dates of satellite images acquisition. In addition, TOA reflectance compensated for variation in Earth–Sun distance between dates.

Relative radiometric normalization technique

Types of vegetation vary in their reflectance values due to the noise caused by atmospheric effects. When conducting change detection and monitoring with multi-temporal images, it is necessary to consider the atmospheric effects of absorption and scattering, solar irradiance, and the noise caused by the detector (Coppin et al. 2004). Thus, it is crucial to normalize these effects. The relative radiometric normalization technique helps to increase the homogeneity between two multi-temporal satellite images (Yuan and Elvidge 1996; Tokola et al. 1999; Lu et al. 2004; Nelson et al. 2005). It is applied to find a linear relationship between two satellite images for DNs, radiance, TOA, or surface reflectance values. Output obtained from this technique is useful in change detection analyses, particularly with NDVI analysis. Through linear regression analysis, the other images are normalized to the reference image in terms of reflectance (Vicente-Serrano et al. 2008). The selection of a reference image should choose the most recent image that is least affected by clouds or atmospheric effects. The relationship between the reference and normalized images is as follow:

$$\rho_{reference,\lambda} = a + b\rho_{normalised,\lambda} \quad (3)$$

where $\rho_{references,\lambda}$ is the reflectance value for the reference image $\rho_{normalised,\lambda}$ is the subject image that is to be normalized, a is the slope or gain and b is the intercept or offset.

Relative radiometric normalization often involves the selection of ground targets, otherwise known as PIFs, which are chosen on the assumption that their reflectance values are constant over the study period. Selection of PIFs often requires the expertise and local knowledge of the analyst (Janzen et al. 2006). Any mistake will affect the accuracy of the results, resulting in a poor correlation between the two different images after regression. Normally, the misinterpretation is caused by atmospheric effects and the noise of the sensor itself. To complete the

Table 1 Summary of the relative radiometric normalization acquired after regression analysis

Satellite images	Equation	Correlation coefficient, R^2
11 January 1991 was normalized to 17 January 2002 -red band (band 3)	$Y=0.964X-0.020$	0.852
11 January 1991 was normalized to 17 January 2002 -NIR band (band 4)	$Y=0.768X-0.059$	0.859

task, several criteria should be considered when choosing constant targets as PIFs (Schott et al. 1988). Therefore, the following criteria should be taken into consideration:

(1) Targets like water, asphalt, and sand are usually selected as PIFs because their reflectance remains constant for a long time and is less affected by atmospheric effects.
(2) Targets must be found in an area that has minimum vegetation coverage. The reflectance for vegetation may vary or change drastically within the time period of two multi-temporal satellite images.
(3) If possible, targets with a wide range of reflectance values should be to be included (from bright to dark areas).

In this study, the Landsat image acquired on January 17, 2002 (Landsat 7 ETM+) was chosen as the reference image, and an image from January 11, 1991 (Landsat 5 TM) was chosen as the normalized image.

ATCOR3

Usually, the absolute radiometric correction methods that are available only correct for the atmospheric effects of satellite imagery (Janzen et al. 2006).

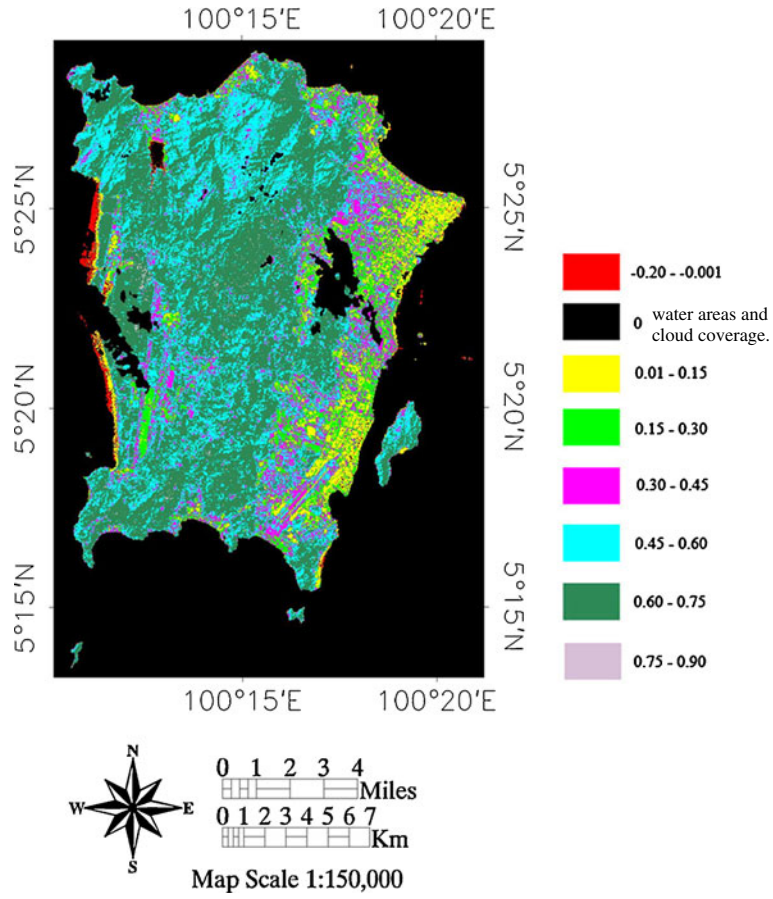

Fig. 2 The map generated based on NDVI computation for 11 January 1991 (normalized image), using relative radiometric normalization

Therefore, they may be suitable in certain flat areas or areas with a specific kind of terrain. However, the proposed algorithm cannot reduce topographic effects. Hence, in mountainous terrain, these methods may introduce some errors while applying the algorithms to eliminate atmospheric effects.

To remove atmospheric and topographic effects efficiently, a method has been developed and implemented for satellite imagery over mountainous areas. The proposed algorithm is based on the Richter model (Richter 1990). It generates a three-dimensional model of the atmosphere by considering the transmittance and radiance functions of areas of different height, including horizontal alterations in atmospheric conditions. Consequently, the algorithm is able to solve the problem of elevation by manipulating the optical depths at different altitudes.

ATCOR3 is a new approach based on the ATCOR2 model, which is implemented in PCI Geomatica 10.1 image processing software. However, the ATCOR2 model was restricted to use with flat terrain for calculating surface reflectance. Both of these models use a dense dark vegetation approach (Liang et al. 1997) and a modified dense dark vegetation approach (Song et al. 2001).

A database containing radiative transfer code is acquired from the calculation of values for direct and diffuse solar flux, path radiance and atmospheric transmittance within a wide range of weather conditions (Richter 1998). Additionally, the ATCOR3 approach requires information, such as slope, orientation and surface elevation, to eliminate topographic effects on data. To be accurate, mountainous terrain should not exceed 3.5 km in height above sea level. Furthermore, if ATCOR3 is applied to areas of rugged terrain, the algorithm needs to calculate the specified atmospheric conditions based on the Lambertian assumption. Overall, the method implemented here is restricted only to high spatial resolution satellite sensors with small swath angles, like Landsat and Systeme pour I'Observation de la Terre.

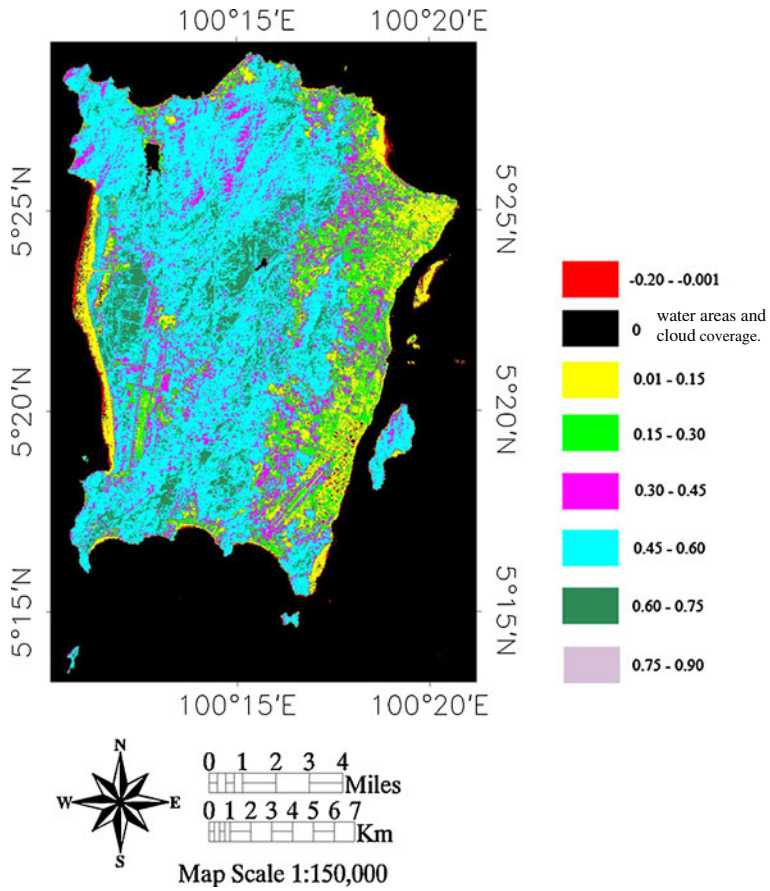

Fig. 3 The map generated based on NDVI computation for 17 January 2002 (reference image), using relative radiometric normalization

Land surface temperature retrieval

To examine the relationship between land surface temperature (LST) and NDVI, LST data were retrieved from the radiometrically and geometrically corrected images using ATCOR3_T with the PCI Geomatica 10.1 image processing software. The advantage of ATCOR3_T is that the module can generate a surface thermal map using reference elevation data. In addition, the retrieval of thematic maps from LST becomes more accurate, especially in high mountain terrain, because it considers the slope and aspect images. In this study, the reference digital elevation model produced from Shuttle Radar Topography Mission (SRTM) data was used to retrieve the LST. In addition, ATCOR3_T also has a built-in function for atmospheric correction, which is only available for band 6 (thermal band) of Landsat images.

NDVI computation

Multi-temporal and multi-spectral satellite images provide useful information for change detection analysis, such as in NDVI computation (Ding et al. 2007; Raynolds et al. 2008). NDVI has been widely used to continuously observe the growth status and spatial density distribution of vegetations (Sun et al. 1998). In addition, vegetation is very sensitive to reflection and absorption in infrared and red bands. Thus, NDVI becomes a good tool to indicate and predict the biomass and greenness in a particular area (Chen and Brutsaert 1998). There are two methods have been proposed to generate thematic maps for NDVI values. One is through the obtained TOA reflectance results (bands 3 and 4) using the relative radiometric normalization technique. The other one is using the method proposed by Rahman and Dedieu (1994) called SMAC. This method correlates the

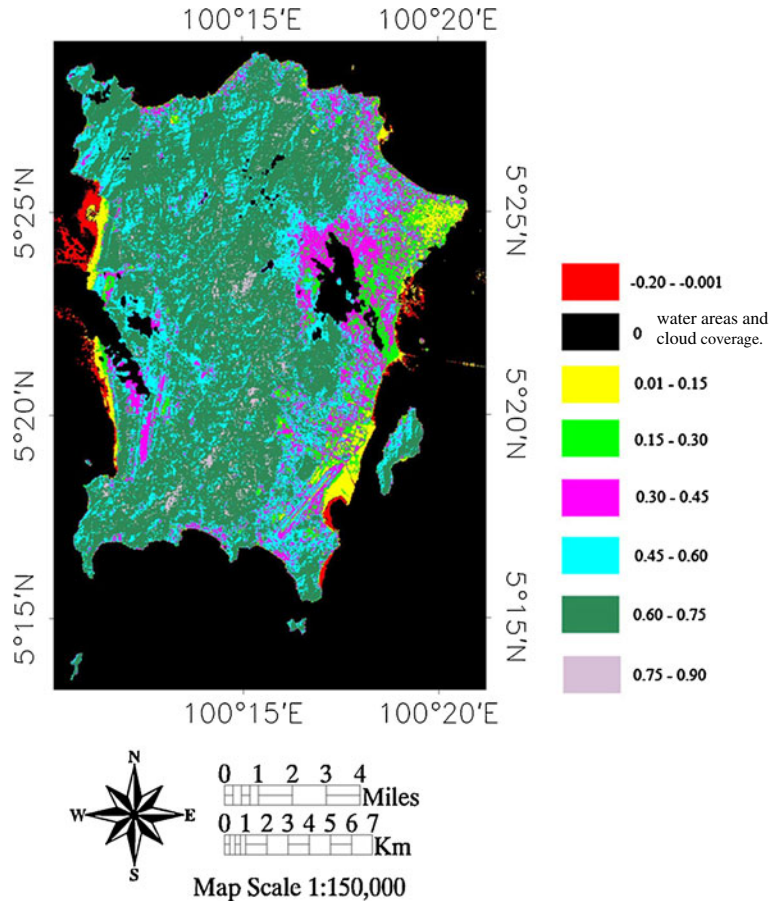

Fig. 4 The map generated based on NDVI computation for 11 January 1991, using SMAC method

TOA reflectivity to at-surface reflectivity with the use of a linear regression correlation. Both of the generated NDVI maps are then compared to one another using both of these methods. In this study, NDVI values for both satellite images were calculated as the ratio between the measured reflectance in the red (R) and near-infrared (NIR) bands based on the following formula (Tucker 1979):

$$\mathrm{NDVI} = (\rho(\mathrm{band4}) - \rho(\mathrm{band3}))/(\rho(\mathrm{band4}) + \rho(\mathrm{band3})) \quad (4)$$

where, ρ is the surface reflectance for band 3 and band 4, respectively.

Cloud masking

Generally, cloud coverage tends to be a problem in the study of optical satellite images (Helmer and Ruefenacht 2007). The situation is worse when the study area is in an equatorial region, like Penang Island. The area of the satellite image that is covered by clouds must be masked out since it will introduce error into the data after processing. Thus, cloud detection techniques are applied to mask out the cloud covered areas. Among all of the cloud detection techniques, two cloud detection tests were selected and carried out to produce satellite images without any cloud coverage.

The cloud masking techniques applied for this study included the ratio of NIR reflectance to visible reflectance and a gross cloud check using brightness temperature (Simpson and Gobat 1996). In daytime and night-time, the gross cloud check uses brightness temperature to detect clouds in the satellite images. However, this technique is only appropriate for certain applications, and is not suitable to detect warm low clouds above the sea. Thus, the alternative cloud detection technique chosen to mask out the cloud area, called the ratio of NIR reflectance to visible reflectance method, was employed. The ratio used in the test is defined as follows (Saunders and Kriebel 1988):

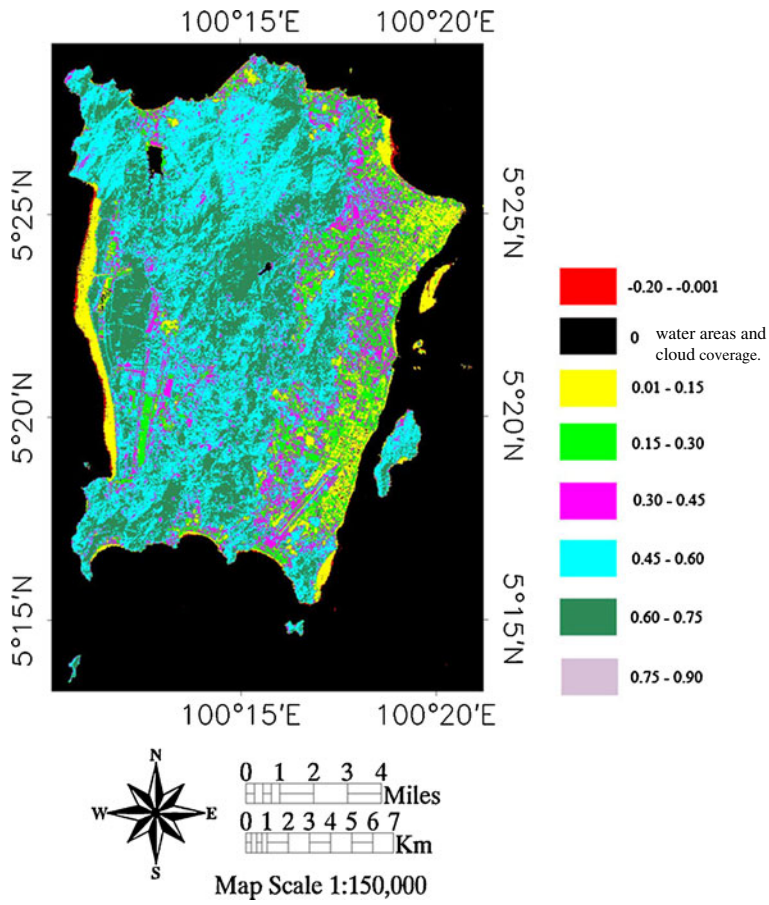

Fig. 5 The map generated based on NDVI computation for 17 January 2002, using SMAC method

Table 2 Summary of the acquired results after regression analysis using SMAC method

Satellite images	Equation	Correlation coefficient, R^2
11 January 1991 (red band)	$Y=1.545X-0.052$	0.870
11 January 1991 (NIR band)	$Y=1.580X-0.091$	0.894
17 January 2002 (red band)	$Y=1.559X-0.086$	0.913
17 January 2002 (NIR band)	$Y=1.145X-0.100$	0.902

$$Q = \frac{R_2}{R_1} \tag{5}$$

where, Q is the ratio between R_2, near-infrared reflectance and R_1, visible reflectance.

To execute the gross cloud check technique, the brightness temperature is required. The assumption is made that the at-sensor brightness temperature of the Earth's surface is a black body, including atmospheric effects. The conversion of the brightness temperature from the at-sensor radiance is given by Chander et al. (2009a; b):

$$T = \frac{K_2}{LN\left[\frac{K_1}{L_\lambda}+1\right]} \tag{6}$$

where

- T Is the effective at-sensor brightness temperature (in Kelvin),
- K_2 Is the calibration constant 2 (in Kelvin)
- K_1 Is the calibration constant 1 [$W/$ (m^2 sr μm)]
- L_λ Is the spectral radiance at the sensor's aperture [W/ (m^2 sr μm)], and
- LN Is the natural logarithm

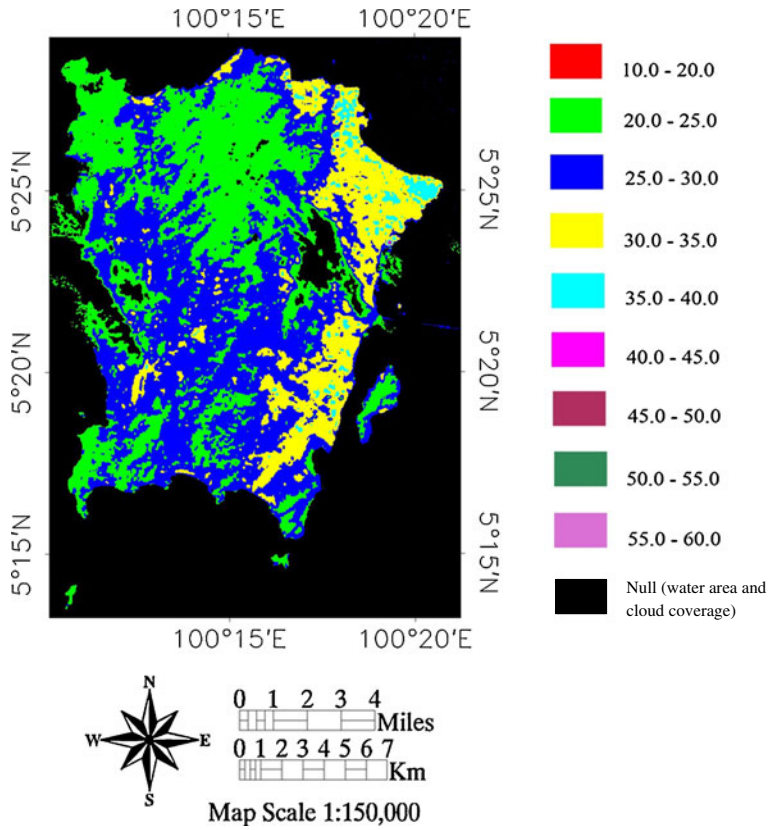

Fig. 6 The maps of LST retrieved using ATCOR3_T for 11 January 1991; the indicator value is in °C

Relationship between NDVI and LST

Two methods were implemented to generate NDVI maps. Both of the Landsat images were used to compare the NDVI values derived from each proposed method. Then, using the LST values retrieved from ATCOR3_T, the relationship between LST and NDVI was investigated within the two different methods. The obtained equation from linear regression analyses was validated with the use of randomly chosen points from the same satellite images. To examine accuracy, the LST value was substituted in the obtained equation to acquire the NDVI value. The resulting NDVI value was then compared with the NDVI value generated using the NDVI map. The average error was calculated between the NDVI value obtained from the equation and the satellite image. To evaluate the value of LST retrieved from the ATCOR3_T and NDVI methods, the error had to be calculated for every single point based on the following equation (Sobrino et al. 2002):

$$\text{Error}(\%) = \frac{\left|\text{NDVI}_{\text{equation}} - \text{NDVI}_{\text{satellite}}\right|}{\text{NDVI}_{\text{satellite}}} \times 100 \quad (7)$$

Results and discussion

NDVI maps in 1991 and 2002

Two satellite images have been generated through the results obtained from the relative radiometric normalization technique. The relative radiometric normalization technique yielded high accuracy, as measured by the linear regression coefficient, R^2, all of which were greater than 0.85 for red and NIR bands. Thus, it can be used to generate NDVI maps from the obtained results of TOA reflectance for bands 3 and 4. Table 1 shows the results acquired from linear regression correlation analyses. Figures 2 and 3 show the NDVI maps for 1991 and 2002, which were generated from Eq. 4.

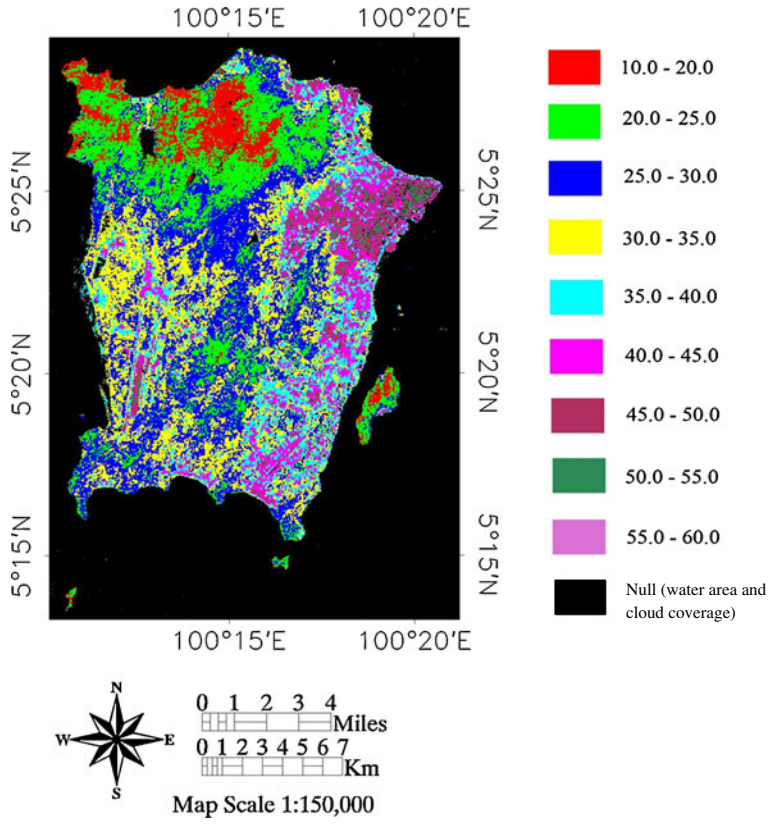

Fig. 7 The maps of LST retrieved using ATCOR3_T for 17 January 2002; the indicator value is in °C

The second method used to generate NDVI values was the SMAC method, proposed by Rahman and Dedieu (1994). The method assumes that the TOA reflectance is linearly correlated with the surface reflectance. In this study, the surface reflectance value was retrieved through ATCOR3 in PCI Geomatica 10.1 image processing software. TOA reflectance was obtained from the data after radiometric calibration for both images. The results show that these parameters are linear correlated with each other. High accuracy was achieved for the regression analysis, since all the correlation coefficients, R^2 were greater than 0.870. Figures 4 and 5 show the NDVI maps for 1991 and 2002, which were generated from SMAC method. Table 2 shows the details for the results of the SMAC method, which was used to generate NDVI maps.

Obviously, both of the proposed method successfully generates NDVI maps for the satellite images on 11 January 1991 and 17 January 2002. Thematic maps generated from NDVI computation show that the NDVI value drastically changed within the study period.

Relationship between LST and NDVI

All satellite images were studied to examine the characteristics of the surface temperature. The thematic maps were generated from the retrieval of LST values using ATCOR3_T in PCI Geomatica 10.1 image processing software. Figures 6 and 7 show the LST maps retrieved using ATCOR3_T for 11 January 1991 and 17 January 2002. From 1991 until 2002, the LST value increased for the study area. There are many reasons caused the increasing value of LST. However, urbanization of the area is the major reason let the LST value to be increased (Tan et al. 2010).

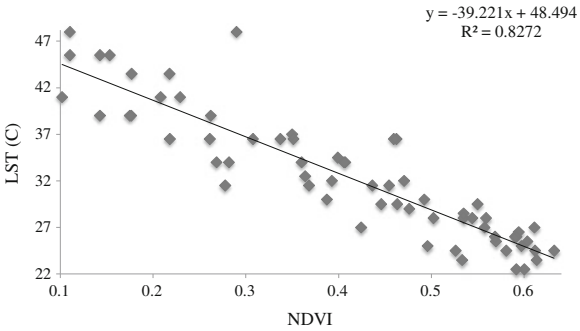

Fig. 9 The relationship between LST and NDVI using the relative radiometric normalization technique for the 17 January 2002 image

The relationship between LST and NDVI was examined using linear regression correlation analysis. NDVI values were generated from the TOA reflectance, using the relative radiometric normalization technique and the SMAC method. The surface reflectance was retrieved from ATCOR3 using PCI Geomatica 10.1 image processing software. Both of the methods yielded high accuracy results since all correlation coefficients, R^2 were greater than 0.8 for regression analysis. Totally 70 points were randomly chosen for the NDVI value at the range from 0.1 to 0.7 for linear regression analysis. The results show that the LST value is negatively correlated with the NDVI value (in linear form). This means that when the LST value increases, the NDVI should decrease, or vice versa (Weng 2001). Figures 8 and 9 show the graphical representations of the NDVI and LST using the relative radiometric normalization technique on

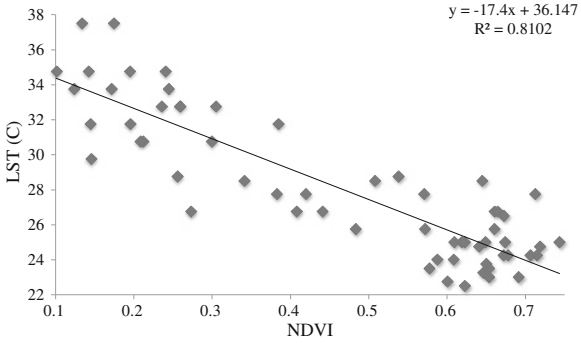

Fig. 8 The relationship between LST and NDVI using relative radiometric normalization technique at 11 January 1991

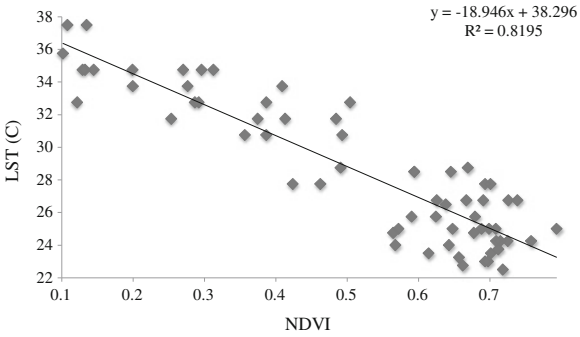

Fig. 10 The relationship between LST and NDVI using the SMAC method for the 11 January 1991 image

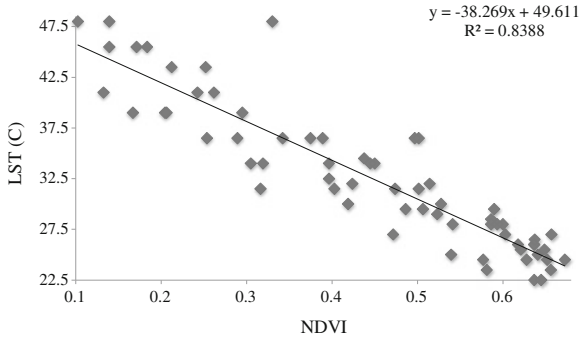

Fig. 11 The relationship between LST and NDVI using the SMAC method for the 17 January 2002 image

images from 11 January 1991 to 17 January 2002. Figures 10 and 11 show the graphical representation of the NDVI and LST using the SMAC method on imagines from 11 January 1991 to 17 January 2002.

Validation of NDVI value

The equation explaining the relationship between LST and NDVI, using both proposed methods to acquire NDVI values was validated with the NDVI value at that particular satellite image. In total, 25 points were randomly chosen from which to substitute LST values in the obtained equation. Then, after obtaining the NDVI value; it was compared with the same chosen point in the NDVI thematic map generated from both of the proposed methods. The average error was calculated for the comparison between NDVI values

Table 3 Comparison between NDVI values (relative radiometric normalization technique) obtained from linear regression analysis and NDVI from the satellite image for 11 January 1991

Number	$NDVI_{equation}$	$NDVI_{satellite}$	$\lvert NDVI_{equation} - NDVI_{satellite} \rvert$	Error (%)
1.	0.7229	0.6620	0.0608	9.1868
2.	0.1978	0.2204	0.0226	10.2667
3.	0.5478	0.5875	0.0397	6.7492
4.	0.6062	0.6092	0.0030	0.5003
5.	0.6645	0.6796	0.0151	2.2148
6.	0.3145	0.3400	0.0255	7.4982
7.	0.4312	0.5182	0.0870	16.7926
8.	0.5478	0.4748	0.0731	15.3938
9.	0.1394	0.1559	0.0164	10.5518
10.	0.1978	0.2314	0.0337	14.5452
11.	0.2561	0.2184	0.0377	17.2690
12.	0.1978	0.2010	0.0032	1.5703
13.	0.0811	0.0721	0.0090	12.4782
14.	0.6499	0.6568	0.0068	1.0428
15.	0.5478	0.5455	0.0023	0.4249
16.	0.6062	0.6869	0.0807	11.7501
17.	0.6645	0.6481	0.0164	2.5270
18.	0.7374	0.7024	0.0351	4.9904
19.	0.6937	0.6627	0.0310	4.6819
20.	0.1978	0.1812	0.0166	9.1608
21.	0.0811	0.0954	0.0143	15.0062
22.	0.0793	0.0758	0.0036	4.7375
23.	0.2561	0.2406	0.0156	6.4729
24.	0.1394	0.1203	0.0191	15.8929
25.	0.3145	0.2826	0.0318	11.2660
Minimum value of the error				0.4249
Maximum value of the error				17.2690
Median value of the error				9.1608
Average of the total error (%)				8.5188

obtained from linear regression analysis and the NDVI value in the satellite image. Tables 3 and 4 show the comparison between NDVI values (relative radiometric normalization technique) obtained from linear regression analysis and NDVI obtained from the satellite images for 11 January 1991 and 17 January 2002 using Eq. 7. Tables 5 and 6 show the comparison between NDVI values (SMAC method) obtained from linear regression analysis and NDVI obtained from the satellite image for 11 January 1991 and 17 January 2002 using Eq. 7. The strong, negative correlation between LST and NDVI implies that the any significant change in LST value can bring the impact on NDVI. Urban expansion does bring up LST by converting vegetation area with non-evaporating materials (Weng 2001). Hence, there will be an error when calculating NDVI value generated from both methods and the value retrieved from satellite image.

The results show that the SMAC method, which is used to generate NDVI thematic maps yielded more consistent results for both of the satellite images in its prediction of the LST value. This is shown by the average of the total error, which, in terms of percentage, predicted the satellite images quite accurately. Although the relative radiometric normalization technique yielded a total error average of less than 6% in 17 January 2002, the value associated with the other satellite image was greater than 8%. Therefore, the SMAC method produced more consistent results

Table 4 Comparison between NDVI values (relative radiometric normalization technique) obtained from linear regression analysis and NDVI from the satellite image for 17 January 2002

Number	$NDVI_{equation}$	$NDVI_{satellite}$	$\lvert NDVI_{equation} - NDVI_{satellite} \rvert$	Error (%)
1.	0.6500	0.64463	0.5000	0.8351
2.	0.4970	0.52294	0.0259	4.9551
3.	0.5735	0.56918	0.0043	0.7618
4.	0.6245	0.63114	0.0066	1.0502
5.	0.5608	0.56545	0.0047	0.8292
6.	0.5990	0.58603	0.0130	2.2168
7.	0.5480	0.52675	0.0213	4.0385
8.	0.6118	0.62732	0.0156	2.4804
9.	0.5863	0.58377	0.0025	0.4271
10.	0.5225	0.50477	0.0178	3.5276
11.	0.6118	0.58147	0.0303	5.2094
12.	0.5225	0.51224	0.0103	2.0089
13.	0.2421	0.20410	0.0380	18.6008
14.	0.1273	0.13114	0.0038	2.9055
15.	0.3058	0.32022	0.0144	4.5008
16.	0.3695	0.41095	0.0414	10.0754
17.	0.1273	0.15601	0.0287	18.3852
18.	0.2421	0.25677	0.0147	5.7276
19.	0.2421	0.24400	0.0019	0.7934
20.	0.2421	0.23688	0.0052	2.1897
21.	0.1273	0.11947	0.0079	6.5808
22.	0.0763	0.08985	0.0135	15.0361
23.	0.1911	0.19714	0.0061	3.0795
24.	0.1273	0.15963	0.0323	20.2353
25.	0.5863	0.54322	0.0430	7.9209
Minimum value of the error				0.4271
Maximum value of the error				20.2353
Median value of the error				3.5276
Average of the total error (%)				5.7748

Table 5 Comparison between NDVI values (SMAC method) obtained from linear regression analysis and NDVI from the satellite image for 11 January 1991

Number	$NDVI_{equation}$	$NDVI_{satellite}$	$\lvert NDVI_{equation} - NDVI_{satellite} \rvert$	Error (%)
1.	0.2925	0.2747	0.0178	6.4817
2.	0.6436	0.6941	0.0505	7.2806
3.	0.6093	0.6485	0.0392	6.0480
4.	0.2925	0.3075	0.0150	4.8771
5.	0.7149	0.6883	0.0265	3.8544
6.	0.6621	0.6237	0.0384	6.1547
7.	0.7413	0.7206	0.0207	2.8664
8.	0.4509	0.4372	0.0137	3.1400
9.	0.7017	0.6787	0.0229	3.3804
10.	0.7017	0.7028	0.0011	0.1521
11.	0.5565	0.5771	0.0206	3.5653
12.	0.2925	0.3252	0.0327	10.0605
13.	0.4509	0.4314	0.0195	4.5105
14.	0.4509	0.4094	0.0415	10.1385
15.	0.0945	0.0979	0.0034	3.5193
16.	0.2397	0.1996	0.0401	20.0837
17.	0.3453	0.3756	0.0303	8.0720
18.	0.2925	0.2636	0.0289	10.9698
19.	0.1869	0.1854	0.0015	0.8205
20.	0.2397	0.2561	0.0164	6.3978
21.	0.1341	0.1247	0.0094	7.5635
22.	0.3981	0.3277	0.0704	21.4761
23.	0.3453	0.3556	0.0103	2.8908
24.	0.2397	0.2563	0.0166	6.4734
25.	0.7149	0.6829	0.0319	4.6758
Minimum value of the error				0.1521
Maximum value of the error				21.4761
Median value of the error				6.0480
Average of the total error (%)				6.6181

in terms of the average percentage error in predicting the LST value.

Conclusion

In this study, an integrated approach of remote-sensing was successfully employed for determining NDVI and LST values from satellite images. The results indicate that Landsat multi-temporal images can provide an accurate map and give detailed descriptions of changes in NDVI and LST from 1991 to 2002.As the few study done before by other researchers, the same relationship for results obtained from this study and their results (Weng 2001). The strong negative correlation between LST and NDVI indicates that the higher the surface temperature, the lower the value of biomass within the study area (Tan et al. 2010). The examined techniques included relative radiometric normalization and the SMAC method, which yielded drastic changes in NDVI values for the satellite images between 11 January 1991 and 17 January 2002.

Using linear regression analysis, both of the radiometric correction methods produced high accuracy NDVI maps for the satellite images. NDVI values generated from both of these methods were also highly linearly correlated with LST values, which were retrieved from ATCOR3_T, using PCI Geo-

Table 6 Comparison between NDVI values (SMAC method) obtained from linear regression analysis and NDVI from the satellite image for 17 January 2002

Number	$NDVI_{equation}$	$NDVI_{satellite}$	$\lvert NDVI_{equation} - NDVI_{satellite} \rvert$	Error (%)
1.	0.6955	0.6446	0.0509	7.8926
2.	0.5387	0.5229	0.0157	3.0095
3.	0.6171	0.5692	0.0479	8.4168
4.	0.6694	0.6311	0.0382	6.0568
5.	0.6040	0.5654	0.0386	6.8219
6.	0.5910	0.6116	0.0210	3.4338
7.	0.5910	0.6281	0.0374	5.9706
8.	0.6563	0.6273	0.0290	4.6188
9.	0.6302	0.5838	0.0464	7.9462
10.	0.5648	0.5662	0.0014	0.2386
11.	0.6563	0.6294	0.0269	4.2690
12.	0.5648	0.5122	0.0526	10.2654
13.	0.2773	0.2904	0.0130	4.4908
14.	0.1597	0.1733	0.0136	7.8435
15.	0.3427	0.3202	0.0224	7.0071
16.	0.4080	0.4110	0.0030	0.7191
17.	0.1597	0.1560	0.0037	2.3613
18.	0.2773	0.2568	0.0205	8.0020
19.	0.5692	0.6103	0.0411	6.7389
20.	0.2250	0.2479	0.0229	9.2299
21.	0.1597	0.1762	0.0165	9.3676
22.	0.1074	0.1224	0.0149	12.2047
23.	0.2250	0.2158	0.0092	4.2673
24.	0.1597	0.1596	0.0065	0.0407
25.	0.6955	0.6084	0.0218	3.5829
Minimum value of the error				0.0407
Maximum value of the error				12.2047
Median value of the error				6.0568
Average of the total error (%)				5.7918

matica 10.1 image processing software. Surface reflectance was retrieved from ATCOR3, which was utilized for SMAC method. ATCOR3 and ATCOR3_T consider both the slope and aspect for LST and surface reflectance retrieval. Validation was performed on the obtained equation through a linear regression correlation analysis of LST and NDVI. The average total error (in percent) using the NDVI retrieved from the relative radiometric normalization technique for satellite images taken in 11 January 1991 and 17 January 2002, were 8.52% and 5.77%, respectively. The average total error (in %) using NDVI retrieved from the SMAC method for satellite images taken in 11 January 1991 and 17 January 2002, were 6.62% and 5.79%, respectively. The relationship between LST and NDVI was more obvious and highly correlated using the SMAC method, due to lower average errors of both satellite images. This means that more consistent results were obtained from the equation to predict LST value. There is a variation between NDVI obtained from relative radiometric normalization technique and SMAC method due to the uncertainty for NDVI value, for different land cover types (Tan et al. 2010). Measuring the LST value from in situ measurements can be very difficult and time-consuming and can require accurate equipment. Therefore, it is beneficial to predict the LST value from the NDVI and LST values generated from remote-sensing technique and from the obtained equation to relate the two.

For future studies, radiometric corrections techniques will consider water vapor, aerosol absorption and scattering to improve the results of the NDVI. A study done by van Leeuwen et al. (2006) indicated that NDVI values retrieved from satellite images are affected by these parameters. Thus, NDVI computation can become more accurate if all these parameters are considered in generating an NDVI thematic map from satellite images.

Acknowledgment The authors gratefully acknowledge the financial support received from the Digital Elevation Models (DEMs) Studies For Air Quality Retrieval From Remote Sensing Data Grant, account number: 304/PFIZIK/638103 and the Environmental Mapping Using Digital Camera Imagery Taken From Autopilot Aircraft Grant, account number: 305/PFIZIK/613606, with additional support from the USM-RU-PRGS Grant, account number: 1001/PFIZIK/831024. Thanks are also extended to the USM technical staff for their support and cooperation.

References

Ahmad, F., Yahaya, A. S., & Farooqi, M. A. (2006). Characterization and geotechnical properties of Penang residual soils with emphasis on landslides. *American Journal of Environmental Sciences, 2*(4), 121–128.

Canty, M. J., Nielsen, A. A., & Schmidt, M. (2004). Automatic radiometric normalization of multitemporal satellite imagery. *Remote Sensing of Environment, 91*, 441–451.

Chander, G., & Markham, B. (2003). Revised Landsat-5 TM radiometric calibration procedure and postcalibration dynamic ranges. *IEEE Transactions on Geoscience and Remote Sensing, 41*(11), 2674–2677.

Chander, G., Markham, B. L., & Helder, D. L. (2009). Summary of current radiometric calibration coefficients for Landsat MSS, TM, ETM+, and EO-1 ALI sensors. *Remote Sensing of Environment, 113*, 893–903.

Chander, G., Markham, B. L., & Barsi, J. A. (2009). Revised landsat-5 thematic mapper radiometric calibration. *IEEE Geoscience and Remote Sensing Letters, 4*(3), 490–494.

Chen, D., & Brutsaert, W. (1998). Satellite-sensed distribution and spatial patterns of vegetation parameters over a tallgrass prairie. *Journal of the Atmospheric Sciences, 55*, 1225–1238.

Chen, X. L., Zhao, H. M., Li, P. X., & Yin, Z. Y. (2006). Remote sensing image-based analysis of the relationship between urban heat island and land use/cover changes. *Remote Sensing of Environment, 104*, 133–146.

Coppin, P., Jonckheere, I., Nackerts, K., & Muys, B. (2004). Digital change detection methods in ecosystem monitoring: An review. *International Journal of Remote Sensing, 25*(9), 1565–1596.

Ding, M., Zhang, Y., Liu, L., Zhang, W., Wang, Z., & Bai, W. (2007). The relationship between NDVI and precipitation on the Tibetan Plateau. *Journal of Geographical Sciences*. doi:10.1007/s11442-007-0259-7.

Du, Y., Teillet, P. M., & Cihlar, J. (2002). Radiometric normalization of multitemporal high-resolution satellite images with quality control for land cover change detection. *Remote Sensing of Environment, 82*, 123–134.

Eckhardt, D. W., Verdin, J. P., & Lyford, G. R. (1990). Automated update of an irrigated lands GIS using SPOT HRV imagery. *Photogrammetric Engineering and Remote Sensing, 56*, 1515–1522.

Furby, S. L., & Campbell, N. A. (2001). Calibrating images from different dates to like-value counts. *Remote Sensing of Environment, 77*, 186–196.

Helmer, E. H., & Ruefenacht, B. (2007). A comparison of radiometric normalization methods when filling cloud gaps in Landsat imagery. *Canadian Journal of Remote Sensing, 33*(4), 325–340.

Janzen, D. T., Fredeen, A. L., & Wheate, R. D. (2006). Radiometric correction techniques and accuracy assessment for Landsat TM data in remote forested regions. *Canadian Journal of Remote Sensing, 32*(5), 330–334.

Kabbara, N., Benkhelil, J., Awad, M., & Barale, V. (2008). Monitoring water quality in the coastal area of Tripoli (Lebanon) using high-resolution satellite data. *ISPRS Journal of Photogrammetry and Remote Sensing, 63*(5), 488–495.

Kaufman, Y. J. (1988). Atmospheric effect on spectral signature. *IEEE Trans on Geoscience and Remote Sensing, 26*(4), 441–451.

Liang, S., Fallah-Adl, H., Kalluri, S., Jaja, J., Kaufman, Y. G., & Townshend, J. R. G. (1997). An operational atmospheric correction algorithm for Landsat Thematic Mapper imagery over the land. *Journal of Geophysical Research, 102*, 173–186.

Lu, D., Mausel, P., Brondizio, E., & Moran, E. (2004). Change detection techniques. *International Journal of Remote Sensing, 25*(12), 2365–2407.

Lunetta, R. S., & Elvidge, C. D. (1998). *Remote sensing change detection: Environment monitoring methods and applications*. London: Taylor and Francis.

Mather, P. M. (2004). *Computer processing of remotely-sensed images—An introduction* (3rd ed., p. 134). New York: Wiley.

Nelson, T., Wilson, H. G., Boots, B., & Wulder, M. A. (2005). Use of ordinal conversion for radiometric normalization and change detection. *International Journal of Remote Sensing, 26*(3), 535–541.

Rahman, H., & Dedieu, G. (1994). SMAC: A simplified method for the atmospheric correction of satellite measurements in the solar spectrum. *International Journal of Remote Sensing, 15*, 123–143.

Raynolds, M. K., Comiso, J. C., Walker, D. A., & Verbyla, D. (2008). Relationship between satellite-derived land surface temperatures, arctic vegetation types, and NDVI. *Remote Sensing of Environment, 112*, 1884–1894.

Richter, R. (1990). A fast atmospheric correction algorithm applied to Landsat TM images. *International Journal of Remote Sensing, 11*(11), 159–166.

Richter, R. (1998). Correction of satellite imagery over mountainous terrain. *Applied Optics, 37*(18), 4004–4015.

Saunders, R. W., & Kriebel, K. T. (1988). An improved method for detecting clear sky and cloudy radiances from AVHRR

data. *International Journal of Remote Sensing, 9*, 123–150.

Schott, J. R., Salvaggio, C., & Volchok, W. J. (1988). Radiometric scene normalization using pseudoinvariant features. *Remote Sensing of Environment, 26*, 1–16.

Schroeder, T. A., Cohen, W. B., Song, C., Canty, M. J., & Yang, Z. (2006). Radiometric correction of multi-temporal Landsat data for characterization of early successional forest patterns in western Oregon. *Remote Sensing of Environment, 103*, 16–26.

Simpson, J. J., & Gobat, J. I. (1996). Improved cloud detection for daytime AVHRR sense over land. *Remote Sensing of Environment, 55*, 21–49.

Sobrino, J. A., Jiménez-Muñoz, J. C., Labed-Nachbrand, J., & Nerry, F. (2002). Surface emissivity retrieval from Digital Airborne Imaging Spectrometer data. *Journal of Geophysical Research, 107*(D23), 4729. doi:10.1029/2002JD002197.

Song, C., Woodcock, C. E., Seto, K. C., Lenney, M. P., & Macomber, S. A. (2001). Classification and change detection using Landsat TM data: When and how to correct atmospheric effects? *Remote Sensing of Environment, 5*, 230–244.

Sun, H., Wang, C., & Niu, Z. (1998). Analysis of the vegetation cover change and the relationship between NDVI and environment factors by using NOAA time series data. *Journal of Remote Sensing, 2*(3), 205–210.

Sun, Z., Ma, R., & Wang, Y. (2008). Using Landsat data to determine land use changes in Datong basin, China. *Journal of Environmental Geology*. doi:10.1007/s00254-008-1470-2.

Tan, K. C., Lim, H. S., MatJafri, M. Z., & Abdullah, K. (2010). Landsat data to evaluate urban expansion and determine land use/land cover changes in Penang Island, Malaysia. *Environmental Earth Science, 60*, 1509–1521.

Tokola, T., Lofman, S., & Erkkila, A. (1999). Relative calibration of multitemporal landsat data for forest cover change detection. *Remote Sensing of Environment, 68*, 1–11.

Tucker, C. J. (1979). Red and photographic infrared linear combinations for monitoring vegetation? *Remote Sensing of Environment, 8*, 127–150.

van Leeuwen, W. J. D., Orr, B. J., Marsh, S. E., & Hermann, S. M. (2006). Multi-sensor NDVI data continuity: Uncertainty and implications for vegetation monitoring applications. *Remote Sensing of Environment, 100*, 67–81.

Vicente-Serrano, S. M., Perez-Cabello, F., & Lasanta, T. (2008). Assessment of radiometric correction techniques in analyzing vegetation variability and change using time series of Landsat images. *Remote Sensing of Environment, 112*, 3916–3934.

Weng, Q. (2001). A remote sensing-GIS evaluation of urban expansion and its impact on surface temperature in the Zhujiang Delta, China. *International Journal of Remote Sensing, 22*(22), 1999–2014.

Yuan, D., & Elvidge, C. D. (1996). Comparison of relative radiometric normalization techniques. *ISPRS Journal of Photogrammetry and Remote Sensing, 51*, 117–126.